Applied Thermal Engineering 218 (2023) 119388

Contents lists available at ScienceDirect

Applied Thermal Engineering

journal homepage: www.elsevier.com/locate/apthermeng

Research Paper

Optimal design of E-type coaxial thermocouples for transient heat measurements in shock tunnels

Li Qi, Guilai Han *, Zonglin Jiang

State Key Laboratory of High-Temperature Gas Dynamics, Institute of Mechanics, Chinese Academy of Sciences, Beijing 100190, China
School of Engineering Science, University of Chinese Academy of Sciences, Beijing 100049, China

ARTICLE INFO

Keywords:
Coaxial thermocouples
Lateral heat conduction
Maximum temperature point
Optimal design
Numerical simulation

ABSTRACT

Coaxial thermocouples have been widely used for transient heat transfer measurements in high-enthalpy shock tunnels. The one-dimensional semi-infinite heat conduction theory is typically used for temperature data processing. However, lateral heat transfer occurs due to material differences between the two electrodes and the junction, causing a deviation in the heat flux measurement from the prediction results of the one-dimensional semi-infinite heat conduction theory. Thus, the lateral heat conduction effect should be investigated to improve the accuracy and reliability of heat flux measurements. In this paper, the heat transfer in E-type (Chromel-Constantan) coaxial thermocouples was analyzed by numerically solving the two-dimensional axisymmetric heat conduction equation with the Du Fort-Frankel scheme. The maximum temperature point on the surface of the coaxial thermocouples shifted to the positive electrode during the heating process. The numerical simulation indicated that the surface temperature of the coaxial thermocouples and the derived heat flux were larger than the theoretical value. The heat flux measurement error of the coaxial thermocouples can be reduced by increasing the width of the positive electrode. Hence, 13 combinations of the diameters of positive electrode and negative electrode were designed for analysis. With the increase of positive electrode diameter or decrease of negative electrode, the heat flux measurement error kept on decreasing, which can be lower than 0.5% in some cases. The results of this study can provide a reference for the design and optimization of coaxial thermocouples.

1. Introduction

An aircraft flying in the atmosphere at supersonic or hypersonic speeds, the incoming air is strongly compressed by the aircraft, and the friction between the aircraft's surface and the air causes a sharp increase in the air temperature. The surface heat flux of the aircraft increases the structure's temperature and causes significant thermal stress on the aircraft, potentially resulting in damage. Therefore, it is crucial to obtain accurate surface heat flux measurements [1–3]. Instantaneous or long-term heat flux measurements can be obtained in a hypersonic, high-enthalpy shock wave wind tunnel using various sensors. Coaxial thermocouples and thin-film resistive temperature gauges are typically used for millisecond-level pneumatic heating processes [4–6], whereas Gardon gauges are used for long-term measurements. Coaxial thermocouples have a simple structure, resist erosion, and possess high measurement accuracy; thus, they are widely used in transient heat flux measurements [7–11]. Coaxial thermocouples provide direct measurements of the surface temperature. The surface heat flux is a typical parameter used to measure the aerodynamic thermal environment of the aircraft surface. The correlation between the surface temperature and heat flux can be determined by the one-dimensional semi-infinite heat conduction theory [12] as follows:

$$T(t) = T(0) + \frac{1}{\sqrt{\rho c k \pi}} \int_0^t q(\tau)(t-\tau)^{-\frac{1}{2}} d\tau \tag{1}$$

where t denotes the time, $T(t)$ denotes the surface temperature and its evolution under aerodynamic heating, $T(0)$ denotes the initial temperature, ρ denotes the density of the material, c denotes the specific heat capacity, k denotes the coefficient of thermal conductivity, and $q(t)$ denotes the aerodynamic heating rate. Equation (1) can also be written in the inverse form to determine $q(t)$ by $T(t)$.

Bendersky [13] first proposed a structural design of coaxial thermocouples in 1953. The accuracy and stability of coaxial thermocouple measurements have been significantly improved in the following

* Corresponding author at: State Key Laboratory of High-Temperature Gas Dynamics, Institute of Mechanics, Chinese Academy of Sciences, Beijing 100190, China.
E-mail address: hanguilai@imech.ac.cn (G. Han).

https://doi.org/10.1016/j.applthermaleng.2022.119388
Received 3 May 2022; Received in revised form 21 September 2022; Accepted 23 September 2022
Available online 28 September 2022

Nomenclature

$T(t)$, $T(0)$	surface temperature at t and $t = 0$ instant in one-dimensional theory, K
$q(t)$	surface heat flux at t instant in one-dimensional theory, MW·m^{-2}
ρ	density of material, kg·m^{-3}
c	specific heat of material, J·kg^{-1}·K^{-1}
k	thermal conductivity coefficient, W·m^{-1}·K^{-1}
$\alpha = k/\rho c$	m^2·s^{-1}
$\beta = (\rho ck)^{1/2}$	W·s$^{0.5}$·m^{-2}·K^{-1}
x, r	coordinate system in physical space, m or mm
$T(x,r)$	temperature field, K
A	coefficient to distinguish 2D planar and axisymmetric cases
ξ, η	coordinate system in computational space
Δt	time step for numerical simulations, s or ms
Δx	scale of grid meshes, m or mm
t_n, t_i	time instant for data in experiments or simulations, s or ms
T^n, T^i	surface temperature at different instant in experiments or simulations, K
δ	depth of heat transfer, m or mm

shock tube calibration was lower than that of water droplet calibration. The difference in thermal diffusivity for different polishing methods was attributed to the junction. A surface junction was investigated to determine the influence of the junction geometry on the response characteristics of coaxial thermocouples [21–23]. Straubinger et al. observed that a larger hot spot radius, thicker insulation, and insulation types with a large thermal mass slowed down the heating rate of the thermocouple [24,25]. Géczy et al. found that high temperature solder (HTS) and Alu-tape improved profiling reliability and repeatability [26].

A schematic diagram of a coaxial thermocouple is shown in Fig. 1. The positive and negative electrodes consist of different materials and are separated by an insulating layer. The surface of coaxial thermocouples is polished with sandpaper to create a junction. A temperature change occurs when a heat flux is applied to the surface of a coaxial thermocouple and wall. The Seebeck effect [23] occurs, i.e., the two electrodes of the coaxial thermocouple generate a potential difference, which is output by wires connected to the two electrodes and recorded by a sensor. A constant relationship exists between the potential difference and the temperature, and the electrical energy is converted into thermal energy. If the surface temperature is known, the surface heat flux can be obtained according to the one-dimensional semi-infinite heat conduction theory [27,28].

The dynamic method is commonly used for calibrating coaxial thermocouples, including the water droplet [29,30], water immersion [31], laser calibration [32,33], and shock tube calibration methods. The coefficient $\beta = (\rho ck)^{1/2}$ is a critical parameter obtained from the calibration and is used to modify the experimental data. In addition to the above factors, the difference between the temperature measured by the coaxial thermocouples and the temperature obtained from the one-dimensional semi-infinite heat conduction theory is also due to the material and thickness of the two electrodes. Therefore, it is necessary to investigate the lateral heat conduction inside coaxial thermocouples and optimize the sensors to increase the measurement accuracy.

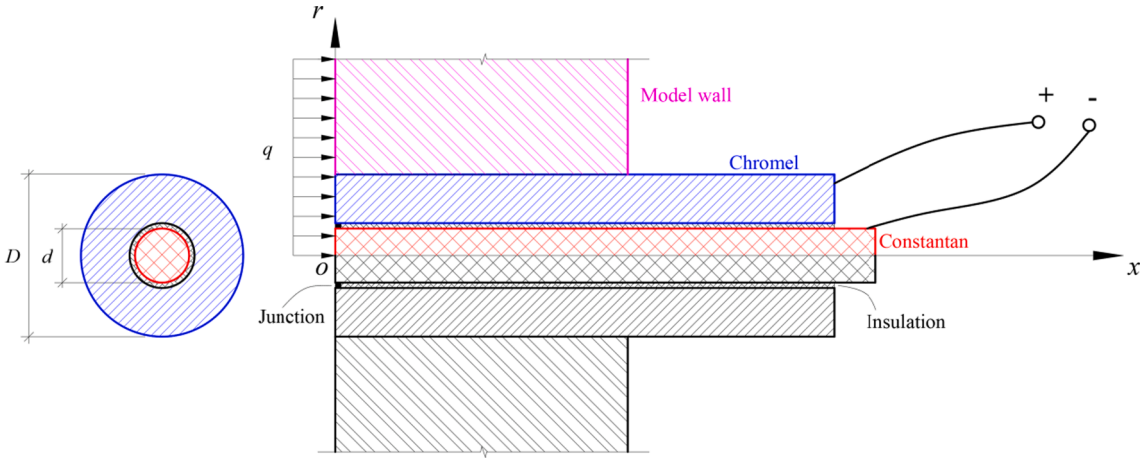

Fig. 1. Schematic of an E-type coaxial thermocouple.

decades. Mohammed et al. [14] conducted microstructure analysis and chemical material characterization of low-cost coaxial thermocouples and evaluated their measurement performance. It was found that the current manufacturing technology was reliable. Sumit et al. [15] used water droplet and water immersion techniques to measure the thermal diffusivity of coaxial thermocouples for millisecond time scales. Goldfeld and Pickalov [16] developed a deconvolution method to improve the signal-to-noise ratio and obtained accurate temperature measurements in a hypersonic wind tunnel. Wang et al. [17] studied the influence of the wall material on the measurements and stated that the lateral heat transfer process should be considered because of differences in the wall material and the physical parameters of coaxial thermocouples. Zhang et al. [18] investigated the influence of the physical parameters of the material and a temperature rise on the heat flux measured by coaxial thermocouples during long-term heating. Pilarczyk and Weglowski [19] calculated the transient temperature fields using inverse heat conduction and analyzed the influence of the time-step selection. Buttsworth [20] observed that the thermal diffusivity coefficient obtained from

During the experimental measurements, several factors can result in lateral heat transfer and effect the measurement accuracy, such as the velocity of gas, radiation [34], local curvature [35], and so on. In this paper, we focused on the lateral heat transfer in the sensors. The response characteristics of coaxial thermocouples were analyzed using numerical simulations of the heat conduction process for 50 ms, which was as long as the efficient test time advanced shock tunnels. The numerical simulation results are compared to results obtained from the one-dimensional semi-infinite heat conduction theory to estimate the error during heat flux measurements. The surface temperature distributions of the coaxial thermocouples at different instants are analyzed to

Table 1
Material parameters of the coaxial thermal couple and experimental model [36].

	Chromel	Constantan	Insulation	Junction	Model wall
ρ/kg·m^{-3}	8730	8920	1060	8825	7930
c/J·kg^{-1}·K^{-1}	447.5	393.1	1960	420.3	500.0
k/W·m^{-1}·K^{-1}	19.25	21.17	0.2	20.21	17.0
α/10^{-6}·m^2·s^{-1}	4.93	6.04	9.62	5.45	4.29
β/W·s$^{0.5}$·m^{-2}·K^{-1}	8672	8616	644.6	8658	8210

ascertain the internal lateral heat conduction. The mechanism is verified by evaluating two examples. According to the lateral heat conduction response, three groups of coaxial thermocouples with thirteen combinations of negative and positive electrode diameters are tested to optimize the sensors and improve the measurement accuracy.

2. Physical model and numerical method

2.1. Construction of coaxial thermocouples

This study used E-type (chromel-constantan) coaxial thermocouples provided by the State Key Laboratory of High-Temperature Gas Dynamics, Institute of Mechanics. The schematic of the coaxial thermocouple is shown in Fig. 1. The positive and negative electrodes of coaxial thermocouples consist of different materials, and a polymer layer is used as insulation between the two electrodes. The electrodynamic potential difference generated by coaxial thermocouples depends on the temperature difference between the junction and the low-temperature end. E-type coaxial thermocouples are composed of a constantan wire and a chromel pipe, with diameters of d and D, respectively. Sandpaper is used at the test end to create the junction that connects the two electrodes. The size of the junction affects the heat flux measurements. We selected the most common junction size. In the simplified model, the width of the junction was the same as the thickness of the insulating layer (10 μm), and the depth of the junction was 12 μm. Since the wall material of the experimental model affects the sensors [17,18], materials with parameters close to that of the electrode material are typically chosen, such as stainless steel (Table 1).

2.2. Governing equations and numerical method

The two-dimensional unsteady heat conduction equation was used as the governing equation to simulate the heat conduction and temperature field in the thermocouples:

$$\rho c\frac{\partial T}{\partial t}=k\left(\frac{\partial^2 T}{\partial x^2}+\frac{\partial^2 T}{\partial r^2}\right)+\frac{A}{r}k\frac{\partial T}{\partial r} \tag{2}$$

where x and r are the coordinate system shown in Fig. 1, $T(x,r,t)$ is the temperature field, t denotes physical time, ρ is the material density, c is the specific heat capacity of the material, k denotes the thermal conductivity of the material, $A = 1$ for two-dimensional axisymmetric cases and $A = 0$ for planar cases.

We used non-dimensionalization and a Jacobian transformation of the governing equation in the computational space:

$$\begin{aligned}\frac{\partial T}{\partial t}&=\left(\xi_x^2+\xi_r^2\right)\frac{\partial^2 T}{\partial \xi^2}+\left(\eta_x^2+\eta_r^2\right)\frac{\partial^2 T}{\partial \eta^2}+2\left(\xi_x\eta_x+\xi_r\eta_r\right)\frac{\partial^2 T}{\partial \xi\partial \eta}\\&+\left(\xi_{xx}+\xi_{rr}\right)\frac{\partial T}{\partial \xi}+\left(\eta_{xx}+\eta_{rr}\right)\frac{\partial T}{\partial \eta}+\frac{A}{r}\left(\xi_r\frac{\partial T}{\partial \xi}+\eta_r\frac{\partial T}{\partial \eta}\right)\end{aligned} \tag{3}$$

The finite difference method was used to discretize the governing equation. The Richardson scheme was the first finite difference scheme for the numerical simulation of a parabolic equation [37]. It uses the second-order central difference to discretize the temporal and spatial terms. O' Brien et al. found that the von Neumann stability condition was not satisfied during the stability analysis of the Richardson scheme [38]. Hence, the Du Fort-Frankel scheme [39] was developed by replacing the spatial parameter with the average of two temporal levels in the spatial discrete. Since the main format of the Richardson scheme was maintained, the scheme is referred to as the improved Richardson scheme. The scheme is implicit and unconditionally stable; it can be expressed and used as an explicit scheme, making the process simple and efficient [40]. For convenience, the Du Fort-Frankel scheme was expressed by discretizing the one-dimensional heat conduction equation $T_t = \alpha T_{xx}$ as follows.

$$T_i^{n+1}=\frac{2\sigma}{1+2\sigma}\left(T_{i+1}^n+T_{i-1}^n\right)+\frac{1-2\sigma}{1+2\sigma}T_i^{n-1} \tag{4}$$

where $\sigma = \alpha\Delta t/\Delta x^2$. The discretization of temporal terms and second order partial differential terms in two dimensional cases can be obtained in each direction individually, and the first order partial differential terms can be discretized by the second order central difference scheme, with detailed formula and corresponding derivation completed by Han and Jiang [40].

The heat flux can be derived from historical surface temperature of the sensors, with an inversed form of Eq. (1). For both experimental and numerical cases, data of the surface temperature can be captured as discrete systems. The data processing [41] for the heat flux can be expressed as follows:

$$q(t_n)=2\sqrt{\frac{\rho ck}{\pi}}\sum_{i=1}^{n}\frac{T^i-T^{i-1}}{\sqrt{t_n-t_i}+\sqrt{t_n-t_{i-1}}} \tag{5}$$

where $q(t_n)$ is heat flux at $t = t_n$, T^i denotes the surface temperature at $t = t_i$.

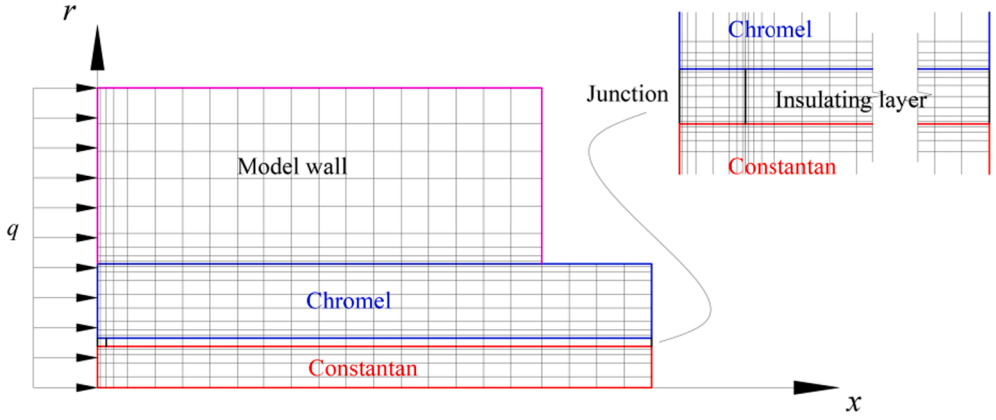

Fig. 2. Schematic of the computational domain and grid mesh.

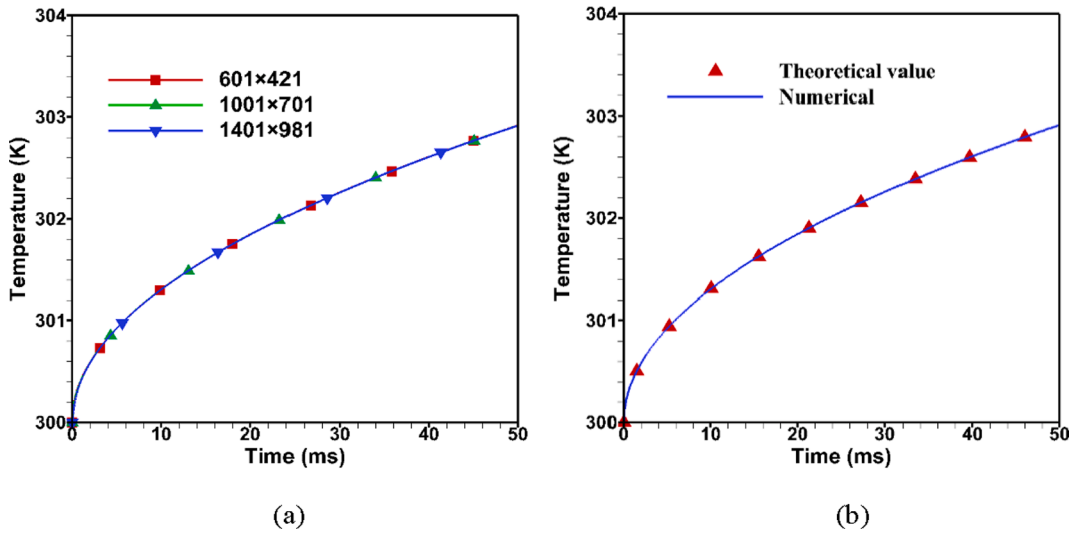

Fig. 3. (a) Grid independence results for the surface temperature evolution with three grid meshes; (b) comparison of numerical and theoretical results of the surface temperature evolution with grid mesh of 1001 × 701.

2.3. Computational domain and boundary conditions

The length of a coaxial thermocouple is typically 20–25 mm. The length of the computational domain in a numerical simulation should be chosen to satisfy the one-dimensional semi-infinite heat conduction theory to reduce the calculation complexity. Hightower et al. [28] proposed the following equation to describe the increase in the depth of heat transfer over time for an infinite column with the heating source at the end:

$$\delta = \sqrt{\alpha \pi^2 t / \ln(2)} \tag{6}$$

where t denotes the thermal penetration time, δ is the depth of heat transfer, and α is the thermal diffusivity of the plate material. The test time of shock tunnels is usually less than 50 ms. The calculation result shows that δ is much less than 4 mm. Therefore, the one-dimensional semi-infinite heat conduction theory is satisfied when the length of the computational domain is no less than 4 mm, which was chosen for the following simulations.

The computational domain was divided into five parts corresponding to the structure of the coaxial thermocouple, including the model wall, positive electrode (chromel), negative electrode (constantan), junction, and insulating layer, as shown in Fig. 2. A rectangular orthogonal grid mesh was applied to discretize the domain. And the grid meshes were algebraically concentrated to the boundaries of the five parts. A constant and uniform heat flux of $q_0 = 0.1$ MW/m^2 was applied to the surface of the coaxial thermocouple and wall, and the boundary condition was $kT_n = q_0$. The boundary condition on the x-axis was an axisymmetric boundary. The top boundary was an adiabatic wall, and it was assumed that the model was much larger than the sensor. The boundaries between the parts had a continuous temperature and heat flux, i.e., $k_1 T_{n1} = k_2 T_{n2}$. Since the length of the computational domain should be larger than the depth of heat transfer in 50 ms, the right boundaries had a constant temperature to ensure that the one-dimensional semi-infinite theory was satisfied. We chose stainless steel as the material close to the positive electrode to minimize the effect of the material [17,18]. The physical parameters of the materials are listed in Table 1.

2.4. Validation

Preliminary numerical simulations were carried out to validate the algorithm, boundary conditions, data processing method, and program codes. The parameters of the five parts were the same to compare the numerical and theoretical results. Three grid meshes were adopted to

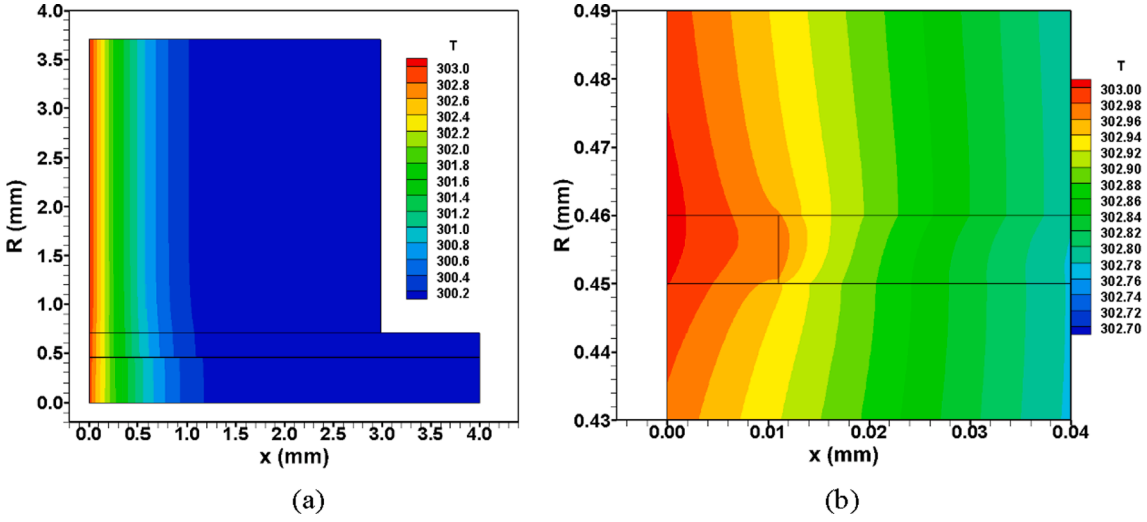

Fig. 4. Temperature contours of (a) the basic model and (b) the area near the junction at 50 ms.

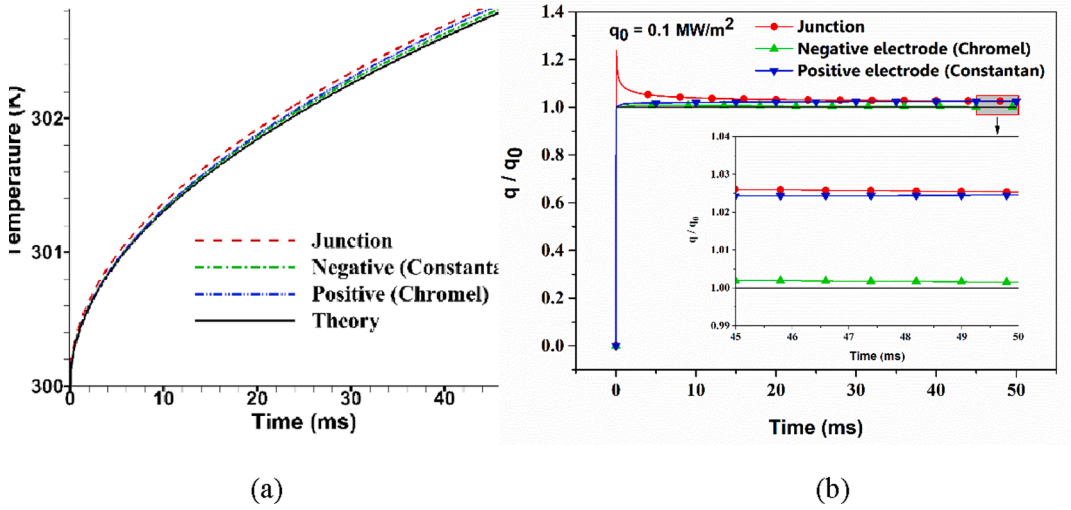

Fig. 5. (a) Temperature increase over time at the three midpoints; (b) normalized heat flux over time at three locations.

check the grid independence with different distribution in x and r direction respectively, including 601 × 421, 1001 × 701 and 1401 × 981. Fig. 3 (a) shows the grid independence results for $q_0 = 0.1$ MW/m^2 on the left boundary and a heating time of 50 ms. The results of the three meshes were in good agreement, verifying the grid independence. The 1001 × 701 grid mesh was chosen for the numerical simulations for convenience. The comparison of the temperature evolution over time for the numerical and theoretical solutions is shown in Fig. 3(b). The good agreement between the numerical and theoretical results indicates the reliability of the algorithm, boundary conditions, data processing, and program codes. Other validation of the physical model and numerical method has been completed by Han and Jiang [40] in 2013.

3. Evolution of the maximum surface temperature

A simulation was carried out with a thermocouple with $D = 1.42$ mm and $d = 0.90$ mm, which are typical values for coaxial thermocouples used in experiments, to investigate the lateral heat conduction and the evolution of the maximum surface temperature. The thickness of the insulating layer was 10 μm, and the thickness of the junction was 12 μm. The thickness and width of the wall were 3.0 mm, and the material was chosen as stainless steel to lower the effect of the wall. A heat flux q_0 of 0.1 MW/m^2 was applied to the surface of the coaxial thermocouple and wall; the heating time was 50 ms, and the initial temperature was 300 K. The main purpose of this manuscript was to optimize the coaxial thermocouple by investigating the lateral heat transfer process and its effect. In experimental measurement, sensors were assumed to capture the maximum temperature on the junction. However, with more detailed information of the temperature field, it is interesting to found that the maximum temperature point moves outside to the boundary of the junction. Hence, it is necessary to describe and explain the details of mechanisms for the coaxial thermocouple optimization in this section.

3.1. Lateral heat conduction

The temperature contours of the entire field and the area near the junction are shown in Fig. 4(a) and 4(b), respectively. Since the distribution is nonuniform in the r direction, the temperature field depicts the lateral heat conduction in the thermocouple. First, the thermal diffusivity α reflects the depth of heat conduction. The larger the value of α, the larger the proportion of heat contributing to heat conduction, and the smaller the proportion of heat contributing to a temperature change. The maximum heat conduction depth is larger inside the positive electrode than inside the negative electrode. Second, the insulating layer prevents the heat transfer from the junction to the insulating layer in the x direction, resulting in overheating at the junction. Therefore, the

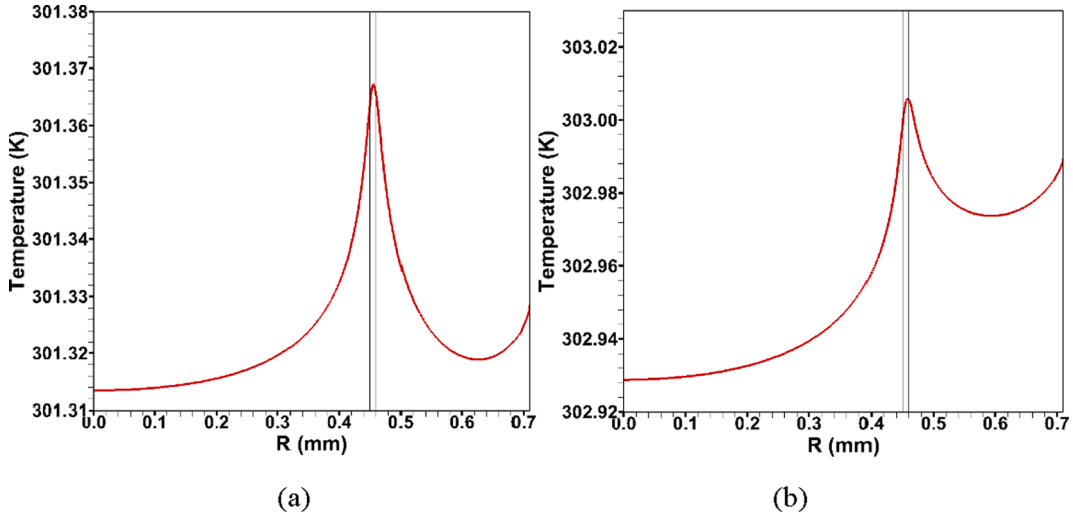

Fig. 6. Temperature on the thermocouple surface at (a) 10 ms and (b) 50 ms.

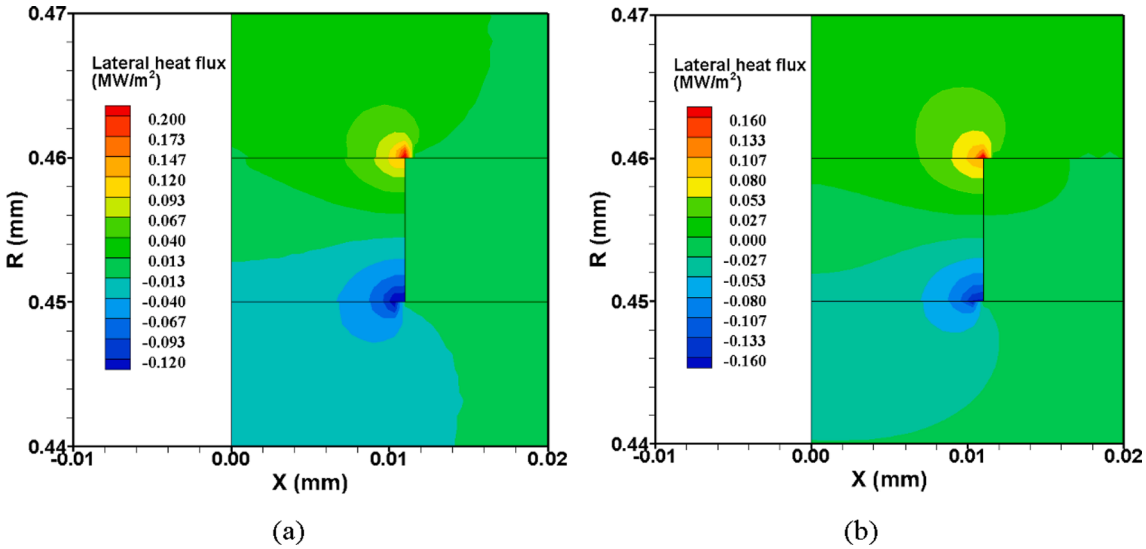

Fig. 7. Contour of lateral heat flux in the thermocouple at (a) 10 ms and (b) 50 ms.

lateral heat conduction in thermocouples is affected by differences in the material parameters, resulting in an error between the numerical result and that obtained from the one-dimensional semi-infinite theory.

The temporal evolution of the temperature at the three midpoints (positive electrode, negative electrode, and junction) obtained from the numerical simulation and the one-dimensional semi-infinite theory is shown in Fig. 5(a). Equation (5) was used to calculate the normalized heat flux data at the three locations, as shown in Fig. 5(b). Normalization (q/q_0) was used to enable the comparison of the heat flux measured by the coaxial thermocouples and obtained from the one-dimensional semi-infinite heat conduction theory. The heat flux at the three midpoints demonstrates the influence of the lateral heat conduction on the heat flux measurement. The measurement errors caused by lateral heat conduction at the midpoint of the junction and the positive electrode are 2.53% and 2.45%, respectively, at 50 ms. In contrast, the error is only 0.15% at the negative electrode. Therefore, it is necessary to investigate the mechanism of lateral heat conduction in coaxial thermocouples to optimize the sensors.

3.2. Evolution of the maximum temperature

The results indicate that the temperature is not uniformly distributed in the r direction due to the lateral heat conduction inside the coaxial thermocouple. The temporal evolution of the temperature differed at the three locations, and the maximum temperature probably occurred at the junction. According to the fundamental principles of coaxial thermocouples, the temperature should be measured at the junction to evaluate the heat flux. However, overheating of the junction might complicate this process. Thus, we captured the maximum temperature on the surface.

The temperature on the coaxial thermocouple surface at 10 ms and 50 ms is shown in Fig. 6(a) and 6(b), respectively. Taking the partial derivative of the temperature field with respect to the r coordinate, and combining with Fourier's law of heat conduction, the lateral heat flux cloud map of the surface of coaxial thermocouples at 10 ms and 50 ms can be obtained, as shown in Fig. 7. It could be seen that there is obvious lateral heat conduction in junction, especially is at the boundary of junction and insulating layer, the lateral heat flux intensity will be greater than the heat flux size q_0 loaded on the surface of coaxial thermocouples.

The maximum temperature on the coaxial thermocouple's surface occurs at the midpoint of the junction surface for a 10 ms heating time, and the curve is relatively symmetrical around this point. However,

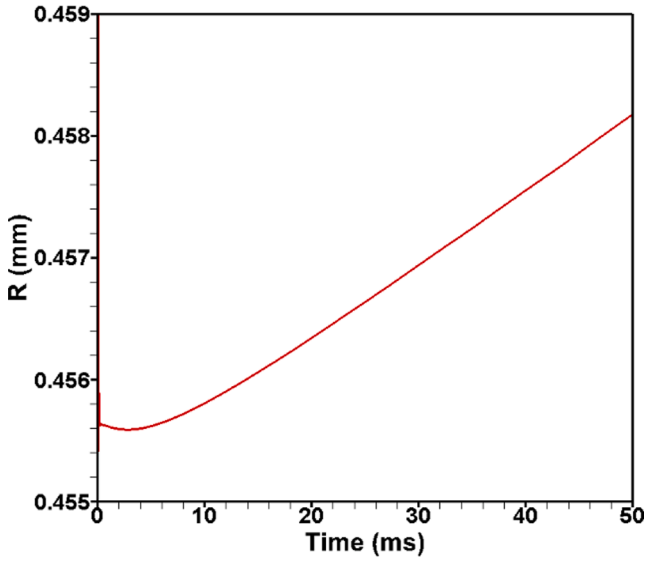

Fig. 8. The movement of the maximum temperature point on the junction.

when the heating time is increased to 50 ms, the location of the maximum temperature shifts to the boundary of the junction and positive electrode due to the lateral heat transfer. The location of the maximum temperature is shown in Fig. 8. It ranges from $r = 0.4556$ mm to $r = 0.4582$ mm during the heating process. The results indicate that the maximum temperature point moves from the middle of the junction surface to the positive electrode surface and to the boundary as the heating time increases to 50 ms.

Since heat conduction is a linear phenomenon, the heat transfer process can be decomposed into two processes, i.e., the lateral heat conduction in the r direction and the longitudinal heat conduction in the x direction. The movement of the maximum temperature point on the junction surface consists of two stages. In the first stage, the inner boundaries between the different materials of the coaxial thermocouple were adiabatic walls for a heating time of 50 ms. Heat conduction occurred in the thermocouple only in the longitudinal direction, resulting in different temperature distributions in the lateral direction. Due to the insulating layer, the temperature of the junction was significantly higher than that of the two electrodes. In the second stage, surface heating stopped, and the boundaries of the junction and the two

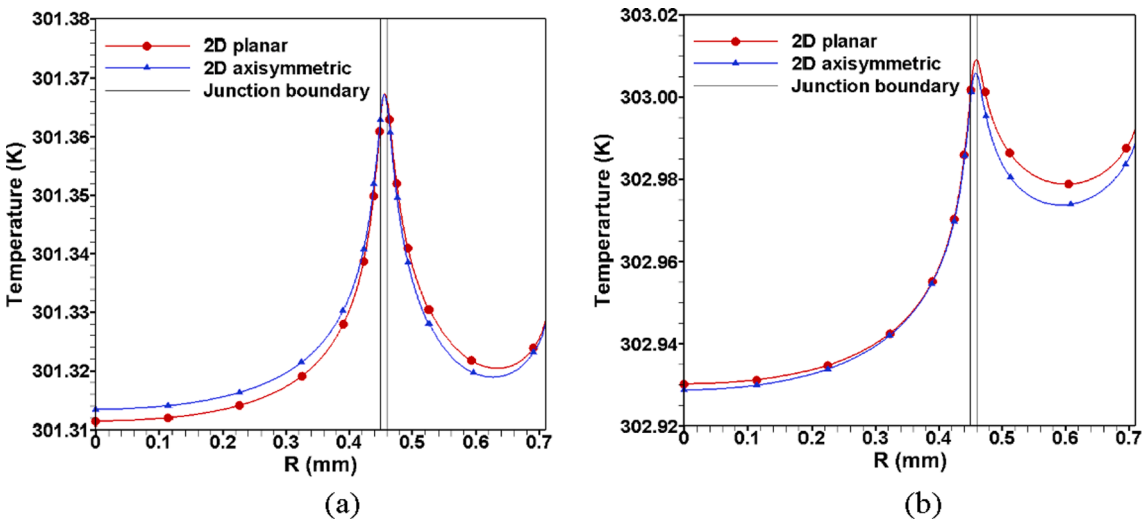

Fig. 9. Temperature on the thermocouple surface for the two-dimensional planar and axisymmetric cases: (a) 10 ms and (b) 50 ms.

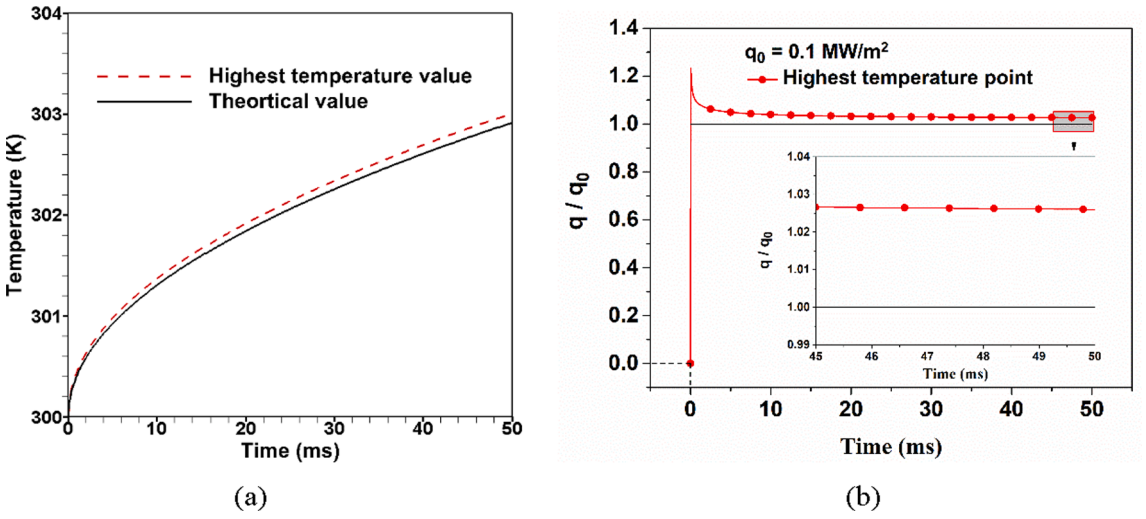

Fig. 10. (a) The maximum temperature on the coaxial thermocouple surface; (b) normalized heat flux obtained from the maximum temperature.

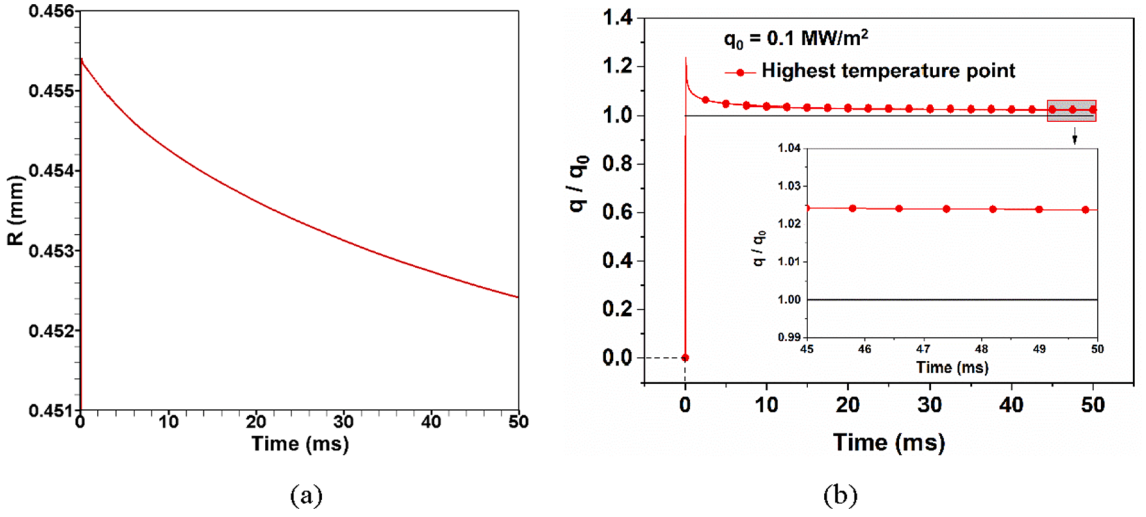

Fig. 11. Results after exchanging the electrode materials: (a) movement of the maximum temperature point on the junction; (b) normalized heat flux obtained from the maximum temperature.

Table 2
Design for different sizes of the positive and negative electrodes of coaxial thermocouples.

d/mm	*D*/mm				
0.50	0.90	1.50	2.10	2.70	3.30
0.90	–	1.50	2.10	2.70	3.30
1.30	–	1.50	2.10	2.70	3.30

electrodes were no longer adiabatic walls. Since the k of Chromel is smaller than that of constantan, less heat is transferred by the electrode with a smaller k value. Thus, the heat loss was lower in the junction area close to the positive electrode than in the area close to the negative electrode. Thus, the maximum temperature location shifted to the positive electrode due to lateral heat conduction.

3.3. Verification of the temperature evolution for a two-dimensional planar case

A two-dimensional planar model was used to illustrate overheating and lateral heat conduction in the area near the junction to understand the shift in the maximum temperature location. The results of the two-dimensional planar and two-dimensional axisymmetric cases at $t = 10$ ms and $t = 50$ ms are shown in Fig. 9(a) and 9(b), respectively. The results of the two cases show similar characteristics and trends, i.e., the maximum temperature point moves toward the positive electrode. It is common to use the maximum temperature point to convert temperature into heat flux. The temporal evolution of the maximum temperature obtained from the numerical simulation and the theory is shown in Fig. 10(a). The temperature measurement error at 50 ms is about 2%. The error of the normalized heat flux caused by lateral heat conduction is about 2.60%, as shown in Fig. 10(b). This error is close to that in Fig. 5 (b), demonstrating that lateral heat conduction is responsible for the evolution of the maximum temperature at the junction.

3.4. Verification of the temperature evolution after exchanging electrode materials

Since the axisymmetric and planar cases were verified, the materials of the two electrodes of the coaxial thermocouple were exchanged, and a numerical simulation of overheating and lateral heat conduction was conducted similarly to the above simulations. After the two electrodes were exchanged, the inside material of the negative electrode was

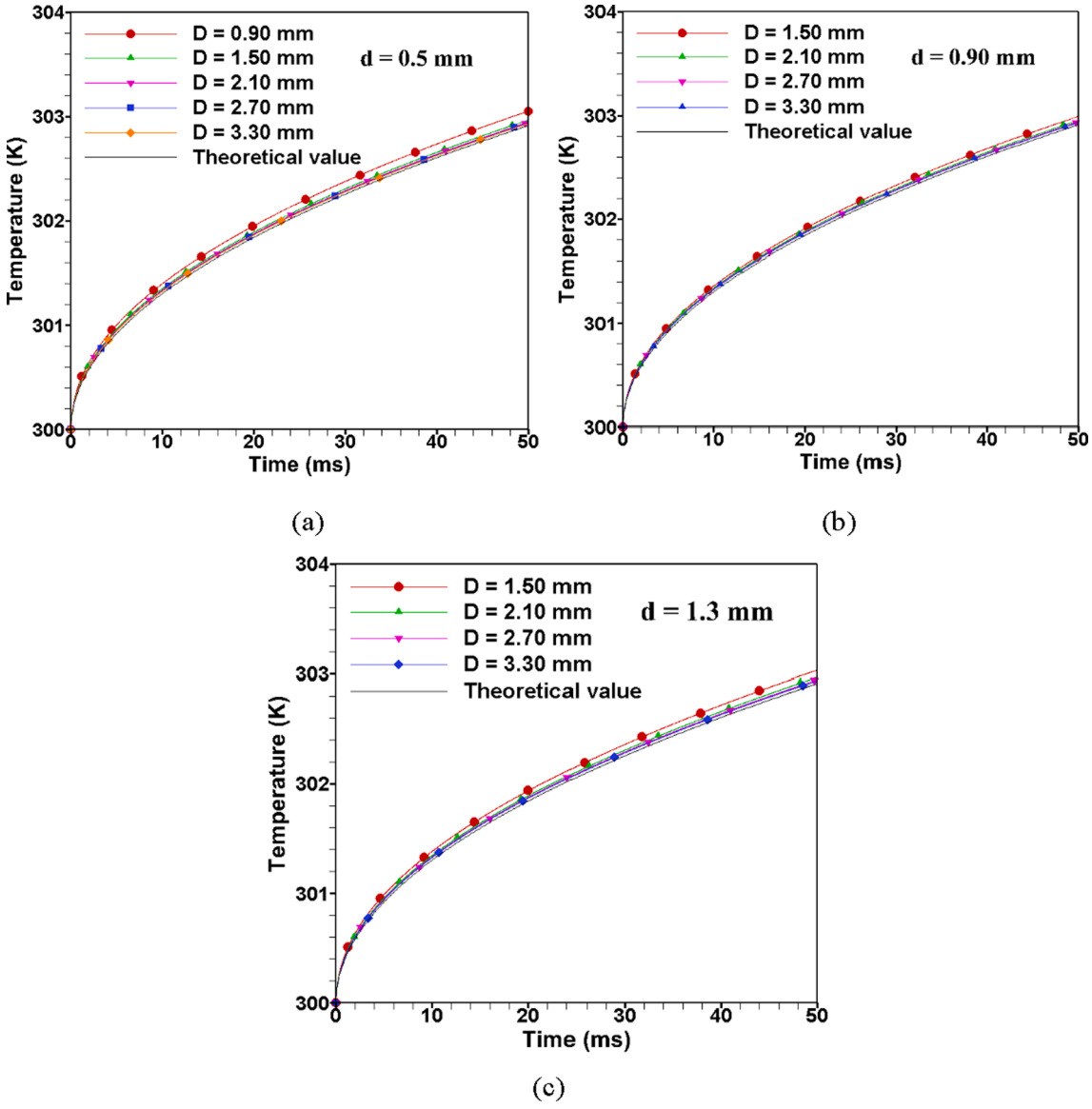

Fig. 12. The maximum temperature on the surface of different coaxial thermocouples with inner diameters of (a) $d = 0.5$ mm, (b) $d = 0.9$ mm, and (c) $d = 1.3$ mm.

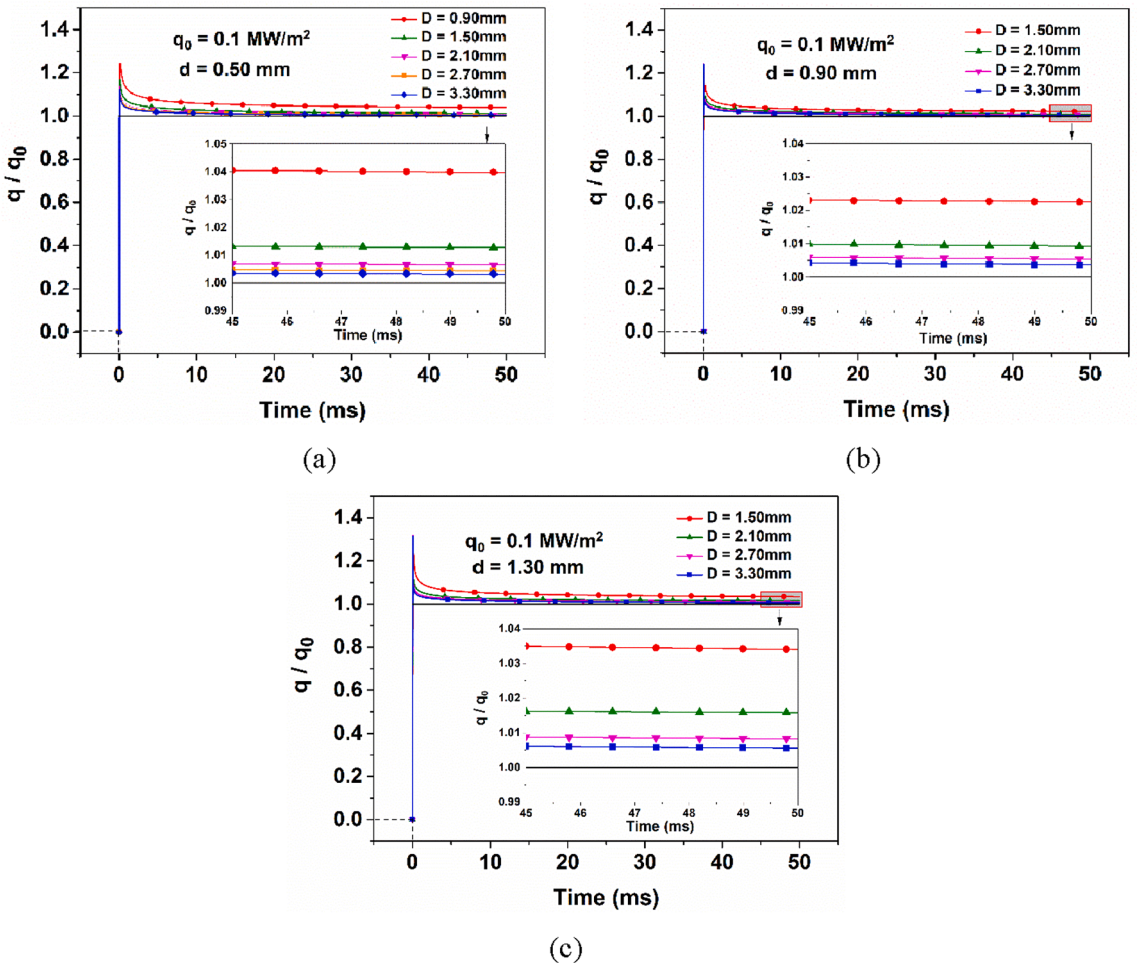

Fig. 13. The normalized heat flux of different coaxial thermocouples with an inner diameter of (a) $d = 0.5$ mm, (b) $d = 0.9$ mm, and (c) $d = 1.3$ mm.

chromel. Hence, the coefficient k was smaller than that of the outside material. The location of the maximum temperature moved to the inside of the electrode as the heating time increased, as shown in Fig. 11(a) with a range of $r = 0.4564$ mm to $r = 0.4524$ mm in 50 ms. The error of the heat flux calculated with the maximum temperature was 2.36% at 50 ms (Fig. 11(b)). Therefore, the mechanism for the lateral heat conduction and the evolution of the maximum temperature points were verified.

4. Optimization of E-type coaxial thermocouples

Simulations were carried out for coaxial thermocouples with $D = 1.42$ mm and $d = 0.9$ mm. The lateral heat conduction in the r direction causes a shift in the maximum temperature point on the junction to the positive electrode (chromel). As mentioned in section 3.1, the heat flux error was only 0.15% using the temperature of the negative electrode. Hence, we decided to optimize the E-type coaxial thermocouple by matching the size of the positive and negative electrodes. The initial conditions, boundary conditions, junction thickness, and insulating layer width remained unchanged, and different sizes of coaxial thermocouples were selected to reduce the heat flux measurement error caused by lateral heat conduction. We used a grid independence test to choose suitable grid sizes and performed numerical simulations on three groups of coaxial thermocouples with 13 different combinations of geometrical sizes. The inner diameters d of thermocouples with three sizes were 0.50 mm, 0.90 mm, and 1.30 mm, and the outer diameter D of thermocouples with five sizes ranged from 0.90 mm to 3.30 mm. The details are listed in Table 2.

Table 3
Heat flux error of coaxial thermocouples with different sizes at 50 ms.

d/mm	D/mm				
	0.90	1.50	2.10	2.70	3.30
0.50	3.98 %	1.28 %	0.65 %	0.43 %	0.32 %
0.90	–	2.26 %	0.93 %	0.54 %	0.37 %
1.30	–	3.41 %	1.58%	0.83 %	0.56 %

The maximum temperature–time curves of the coaxial thermocouple with different sizes of the negative electrode diameter d for a heating time of 50 ms are shown in Fig. 12. The trends of the maximum temperature curves indicate a substantial difference between the numerical simulation and theoretical results. As the outer diameter D of the positive electrode increases, the difference in the temperature decreases for all three groups with different d. Thus, coaxial thermocouples can be optimized by increasing diameter of outer positive electrode and decreasing diameter of inner electrode.

The normalized heat flux derived from the one-dimensional semi-infinite theory for coaxial thermocouples with different inner diameters is shown in Fig. 13. The heat flux error between the numerical and theoretical results decreases with an increase in the outer diameter D of the positive electrode for all three groups in agreement with Fig. 12. The errors at 50 ms are listed in Table 3. For each group of d, the largest errors in heat flux happened with the smallest D, and the smallest errors happened with largest D. The two largest heat flux errors (greater than3.5%) occur for ($d = 0.50$ mm, $D = 0.90$ mm) and ($d = 1.30$ mm, $D = 1.50$ mm), and the error is less than 1.0% for $D \geq 2.10$ mm and $d \leq$

0.90 mm. The error is approximately 0.50% for $D \geq 2.70$ mm and $d \leq 0.90$ mm, much lower than for sensors with D around 1.5 mm and d around 0.9 mm. The tendency for the error varied with d and D can be regarded as, the smaller d and the larger D were, the smaller the discrepancy was, as shown in Table 3. However, the smaller d and larger D will lead to other problems in manufacturing and installation of sensors. Hence, the optimal design for the coaxial couples might be $d \leq 0.90$ mm and D around 3.0 mm, which will keep the error no more than 0.50%.

Our results indicate that the accuracy of the measured heat flux increase and the sensitivity of the measurement error to the diameter decreases with an increase in the diameter of the positive electrode. According to Equation (6), the maximum heat transfer depth of the positive electrode material is approximately 2.9 mm at a heating time of 50 ms. Some of the heat was conducted laterally from the junction area to the positive electrode and contributed to the temperature rise, and some of the heat was conducted in the longitudinal direction. In the range of the maximum heat transfer depth, the larger the positive electrode and the smaller the negative electrode, the more heat is transferred from the junction area to the positive electrode, resulting in a decrease in temperature of the junction area and a reduction in the measurement error caused by lateral heat conduction. If the diameter of the negative electrode is small and the diameter of the positive electrode exceeds the maximum heat transfer depth, the heat transferred from the junction area to the positive electrode does not increase significantly, reducing the sensitivity of the measurement error to the diameter of the positive electrode. Therefore, coaxial thermocouples can be optimized by changing the diameter to reduce the measurement error.

5. Conclusion

Coaxial thermocouples are commonly used as heat sensors in shock tunnels to measure the surface temperature and convert it into heat flux using the one-dimensional semi-infinite theory. However, lateral heat conduction occurs due to differences in the physical parameters of the materials. In this study, lateral heat conduction and its effect on the measurement error were numerically simulated using E-type coaxial thermocouples and a heating time of 50 ms. It was found that overheating of the junction resulted in temperatures significantly higher than that of the two electrodes. The maximum temperature location on the surface shifted from the middle of the junction to the positive electrode. We tested coaxial thermocouples using 13 combinations of negative and positive electrode diameters to minimize the effect of lateral heat conduction. The optimized coaxial thermocouples had a much lower heat flux error (approximately 0.5%) than typical thermocouples ($D \approx 1.5$ mm, $d \approx 0.9$ mm), which have an approximate heat flux error of 2.26%. The manufacturing process might require changes to increase the outer diameter of the positive electrode, although this is not a complex operation. The calibration of the optimized sensors and their use for aerodynamic heating will be discussed in a future study.

Declaration of Competing Interest

The authors declare that they have no known competing financial interests or personal relationships that could have appeared to influence the work reported in this paper.

Data availability

Data will be made available on request.

Acknowledgments

This work was supported by the National Key Research and Development Program of China (2019YFA0405204 and 2016YFA0401201) and the National Natural Science Foundation of China (12132017, 11872066, and 11727901).

References

[1] B.R. Hollis, S. Borrelli, Aerothermodynamics of blunt body entry vehicles, Prog. Aerosp. Sci. 48–49 (2012) 42–56.
[2] S.L. Gai, N.R. Mudford, Stagnation point heat flux in hypersonic high enthalpy flow, Shock Waves 2 (1) (1992) 43–47.
[3] J.A. Fay, F.R. Riddell, Theory of stagnation point heat transfer in dissociated air, Aeronaut Sci. 25 (1958) 73–85.
[4] K.J. Irimpan, N. Mannil, H. Arya, V. Menezes, Performance evaluation of coaxial thermocouple against platinum thin film gauge for heat flux measurement in shock tunnel, Measurement 61 (2015) 291–298.
[5] J.I. Frankel, M. Keyhani, Theoretical development of a new surface heat flux calibration method for thin-film resistive temperature gauges and co-axial thermocouples, Shock Waves 23 (2) (2013) 177–188.
[6] Y. Liu, Y. Mitsutake, Y. Mitsutake, M. Monde, Development of fast response heat transfer measurement technique with thin-film thermocouples, Int. J. Heat Mass Transf. 162 (2020), 120331.
[7] S.L.N. Desikan, K. Suresh, K. Srinivasan, P.G. Raveendran, Fast response co-axial thermocouple for short duration impulse facilities, Appl. Therm. Eng. 96 (2016) 48–56.
[8] K. Srinivasan, S.L.N. Desikan, R. Saravanan, A. Kumar, P.K. Maurya, Fore-body and base heat flux measurements on a typical crew module in short duration impulse facilities, Appl. Therm. Eng. 103 (2016) 842–854.
[9] V. Menezes, S. Bhat, A coaxial thermocouple for shock tunnel applications, Rev. Sci. Instrum. 81 (10) (2010) 104905.
[10] S.K. Manjhi, R. Kumar, Performance analysis of coaxial thermocouples for heat flux measurement of an aerodynamic model on shock tube facility, Measurement 166 (2020), 108221.
[11] S. Agarwal, N. Sahoo, K.J. Irimpan, V. Menezes, S. Desai, Comparative performance assessments of surface junction probes for stagnation heat flux estimation in a hypersonic shock tunnel, Int. J. Heat Mass Transf. 114 (2017) 748–757.
[12] D.L. Schultz, T.V. Jones, Heat Transfer Measurements in Short Duration Facilities, Technical Report, AGARD-AG-165, University of Oxford, 1973.
[13] D. Bendersky, A special thermocouple for measuring transient temperatures, Mech. Eng. 75 (2) (1953) 117–121.
[14] H. Mohammed, H. Salleh, M.Z. Yusoff, Design and fabrication of coaxial surface junction thermocouples for transient heat transfer measurements, Int. Commun. Heat Mass Transfer 35 (7) (2008) 853–859.
[15] A. Sumit, S. Niranjan, K. Rishikesh, Experimental techniques for thermal product determination of coaxial surface junction thermocouples during short duration transient measurements, Int. J. Heat Mass Transf. 103 (2016) 327–335.
[16] M.A. Goldfeld, V.V. Pickalov, Application of method of deconvolution at temperature measurements in high-enthalpy impulse wind tunnels, Appl. Therm. Eng. 113 (2017) 731–738.
[17] Q. Wang, H. Olivier, J. Einhoff, J. Li, W. Zhao, Influence of Test Model Material on the Accuracy of Transient Heat Transfer Measurements in Impulse Facilities, Exp. Therm Fluid Sci. 104 (2019) 59–66.
[18] S. Zhang, Q. Wang, J. Li, X. Zhang, H. Chen, Coaxial Thermocouples for Heat Transfer Measurements in Long-Duration High Enthalpy Flows, Sensors 20 (18) (2020) 52–54.
[19] M. Pilarczyk, B. Weglowski, Determination and validation of transient temperature fields within a cylindrical element using the inverse heat conduction method, Appl. Therm. Eng. 150 (2019) 1224–1232.
[20] D.R. Buttsworth, Assessment of effective thermal product of surface junction thermocouples on millisecond and microsecond time scales, Exp. Therm Fluid Sci. 25 (6) (2001) 409–420.
[21] E.C. Marineau, H.G. Hornung, Modeling and Calibration of Fast-Response Coaxial Heat Flux Gages, 47th AIAA Aerospace Sciences Meeting, Orlando, Florida, 2009.
[22] A. Kovacs, R.B. Mesler, Making and Testing Small Surface Thermocouples for Fast Response, Rev. Sci. Instrum. 35 (4) (1964) 485–488.
[23] S.R. Sanderson, B. Sturtevant, Transient heat flux measurement using a surface junction thermocouple, Rev. Sci. Instrum. 73 (7) (2002) 2781–2787.
[24] D. Straubinger, B. Illés, D. Busek, N. Codreanu, A. Géczy, Modelling of thermocouple geometry variations for improved heat transfer monitoring in smart electronic manufacturing environment, Case Stud. Therm. Eng. 33 (2022), 102001.
[25] D. Straubinger, B. Illés, R. Berényi, A. Géczy, Simulation of reflow-based heat transfer on different thermocouple constructions, Proceedings of 43nd IEEE-ISSE conference (2020) 1–6.
[26] A. Géczy, B. Kvanduk, B. Illés, G. Harsányi, Comparative Study on Proper Thermocouple Attachment for Vapour Phase Soldering Profiling, SOLDERING & SURFACE MOUNT TECHNOLOGY 28/1 (2016) 7-12.
[27] P. Buro, B. Weigand, One-dimensional heat conduction in a semi-infinite solid with the surface temperature a harmonic function of time: a simple approximate solution for the transient behavior, J. Heat Transfer 112 (4) (1990) 1076–1079.
[28] T.M. Hightower, R.A. Olivares, D. Philippidis, Thermal Capacitance (Slug) Calorimeter Theory Including Heat Losses and Other Decaying Processes, Thermal and Fluids Analysis Workshop (TFAWS), San Jose, CA, USA, 2008.
[29] Y.M. Qiao, S. Chandra, Boiling of droplets on a hot surface in low gravity, Int. J. Heat Mass Transf. 39 (7) (1996) 1379–1393.
[30] K. Han, G. Song, X. Ma, B.o. Yang, An experimental and theoretical study of the effect of suspended thermocouple on the single droplet evaporation, Appl. Therm. Eng. 101 (2016) 568–575.

[31] S. Niranjan, A. Sumit, Experimental techniques for thermal product determination of coaxial surface junction thermocuples during short duration transient measurements, Int. J. Heat Mass Transf. 103 (2016) 327–335.
[32] J.A. Gatowski, M.K. Smith, A.C. Alkidas, An experimental investigation of surface thermometry and heat flux, Exp. Therm Fluid Sci. 2 (3) (1989) 280–292.
[33] Y. Li, Z. Zhang, C. Zhao, X. Hao, N. Dong, W. Yin, Z. Pang, Laser based method for dynamic calibration of thermocouples, Appl. Therm. Eng. 174 (2020) 115276.
[34] Z. Zou, W. Yang, W. Zhang, X. Wang, J. Zhao, Numerical modeling of steady state errors for shielded thermocouples based on conjugate heat transfer analysis, Int. J. Heat Mass Transf. 119 (2018) 624–639.
[35] G. Han, Q. Li, Z. Jiang, Analytic investigation on error of heat flux measurement and data processing for large curvature models in hypersonic shock tunnels, Appl. Mathematics Lett. 134 (2022), 108342.
[36] R.P. Benedict, Manual on the use of thermocouples in temperature measurement, fourth ed., ASTM, New York, 2003, pp. 29–30.
[37] L.F. Richardson, The Approximate Arithmetical Solution by Finite Differences of Physical Problems Involving Differential Equations, with an Application to the Stresses in a Masonry Dam. Philos. Trans. Roy. Soc. London, Ser. A 210 (1910) 307-357, and Proc. Roy. Soc. London, Ser. A 83 (1910) 335-336.
[38] G.G. O'Brien, M.A. Hyman, S. Kaplan, A Study of the Numerical Solution of Partial Differential Equations, Stud. Appl. Math. 29 (1–4) (1950) 223–251.
[39] E.C. Du Fort, S.P. Frankel, Stability Conditions in the Numerical Treatment of Parabolic Differential Equations, Math. Tables Aids Comp. 7 (1953) 135–152.
[40] G. Han, Z. Jiang, Approximate analytic solution of heat conduction in hollow semi-spheres flying at hypersonic speed, Int. Commun. Heat Mass Transfer 43 (2013) 46–52.
[41] B.R. Hollis, User's manual for the one-dimensional hypersonic experimental aero-thermodynamic (1DHEAT) data reduction code, NASA, New York, 1995, pp. 3–8.